IEEE Access
Multidisciplinary | Rapid Review | Open Access Journal

Received December 11, 2019, accepted January 8, 2020, date of publication January 13, 2020, date of current version January 24, 2020.

Digital Object Identifier 10.1109/ACCESS.2020.2966222

Calibration of Motional Frequency Spread for Wide-Band FMCW Automotive Millimeter-Wave Radar

CHENG ZHANG[1,2], (Member, IEEE), MENGDE CAO[1], YUQIN GONG[1], YANG LI[1], YONGMING HUANG[1,2], (Senior Member, IEEE), AND HAIMING WANG[1,2], (Member, IEEE)

[1]School of Information Science and Engineering, Southeast University, Nanjing 210096, China
[2]Purple Mountain Laboratories, Nanjing 210096, China

Corresponding author: Yongming Huang (huangym@seu.edu.cn)

This work was supported in part by the National Natural Science Foundation of China under Grant 61901107 and Grant 61720106003, in part by the Natural Science Foundation of Jiangsu Province under Grant BK20190337, in part by the Research Project of Jiangsu Province under Grant BE2018121, and in part by the Zhishan Young Scholar Program of Southeast University.

ABSTRACT As a key module for self-driving cars and advanced driver assistant systems (ADAS), frequency modulation continuous wave (FMCW) automotive millimeter-wave (mmwave) radar has a good market prospect. Due to the relative motion of target and radar in the detection window, the motional frequency spread is inevitable especially for wide-band FMCW automotive mmwave radar systems with large bandwidth and possible high-speed motion. In this paper, for wide-band FMCW automotive mmwave radar systems, we first derive analytical expressions of the motional frequency interference term and phase interference term in the intermediate frequency (IF) signal. Then, the effect of frequency spread is comprehensively analyzed with the help of numerical results. Motivated by the mechanism and influence of frequency spread, we propose three schemes for motional frequency spread calibration with different performance-complexity tradeoff. Finally, simulations verify that the proposed schemes can effectively compensate the degradation of system resolution and parameter estimation accuracy due to frequency spread.

INDEX TERMS Automotive radar, calibration, frequency spread, millimeter-wave, wide-band FMCW.

I. INTRODUCTION

Automotive millimeter-wave (mmwave) radars were first deployed several decades ago, and the fist-stage development was mainly limited by electronic components. With the advancement of integrated circuits, artificial intelligence and self-driving, the research on automotive mmwave radars including circuit implementation, market analysis and signal processing have become active in recent years [1]–[4]. The evolution of automotive mmwave radars from their inception to the present was introduced in [5].

Mmwave radars have excellent range resolution, high range accuracy, and good sensibility to the velocity of targets. Under almost all weather conditions, mmwave radars can guarantee a certain level of performance [6]. Simultaneously, with highly integrated and inexpensive mmwave circuits implemented in silicon, mmwave radars are perfectly adapted to the limitations and requirements of small size, low power and low cost on the sensors in the self-driving systems [7]. Therefore, mmwave radars have significant advantages and irreplaceable functions compared to other sensors, e.g., laser radar, ultrasonic radar and camera, in the fields of self-driving and advanced driver assistant systems (ADAS).

The waveforms of the automotive mmwave radar include continuous wave (CW), pulse continuous wave, frequency modulation continuous wave (FMCW) and stepped frequency continuous wave (SFCW). Each waveform has its own applicable situation due to its specific performance metrics including range and velocity resolution. The various waveforms of automotive mmwave radar for signal processing and their performance have been summarized in [8]. FMCW, also known as linear frequency modulation continuous wave (LFMCW), is widely used in automotive industry due to its simplicity in the signal generation and processing. In FMCW radars, targets are separated via using the frequency difference between the transmitted and received

The associate editor coordinating the review of this manuscript and approving it for publication was Xiaoguang Leo Liu.

signals. Meanwhile, high velocity resolution and range resolution can be achievable which are inversely proportional to the sweep interval and bandwidth [9]. In particular, multiple FMCW fast chirps are used to detect multiple targets via exploiting frequency difference in range dimension and the Doppler frequency measured from phase difference of consecutive chirps [8], [10], [11]. Besides, FMCW's ability to discriminate moving objects and stationary clutter can be utilized to solve the problem of moving target classification and recognition in ADAS with the help of machine learning or neural networks [12], [13].

In automotive FMCW radars, the transmitter emits signal continuously. Since the signal duration occupies the whole detection time, the radar range of one target is generally no longer stationary. Specifically, the range migration is not only related to the Doppler-dimension time (slow sampling time) but also associated with the range-dimension time (fast sampling time) [14]. Therefore, the FMCW intermediate frequency (IF) signal has a frequency shift resulted from the relative motion between radar and target. This then causes the frequency spread and affects the overall system performance. For synthetic aperture radar (SAR) systems, the effect of motional frequency spread has been widely studied [15]–[17] where many calibration algorithms was proposed to solve the range migration problem due to the long accumulation time. For FMCW-SAR systems, via utilizing the characteristics that the SAR radar has constant velocity, a calibration algorithm was proposed to compensate the frequency shift both in range time and azimuth Doppler domain [14].

For FMCW automotive mmwave radars, the motional frequency spread phenomenon are generally ignored in the signal processing procedure. The performance degradation can be acceptable in the narrow-band and low-velocity scenario. However, in the scenario with wide bandwidth and high velocity, the motional frequency spread can be very harmful. Compared to SAR radar systems, the application scenario and signal processing procedure of FMCW automotive mmwave radars are both significantly different, and the radar velocity is generally timely variable. Therefore, the algorithm proposed in [14] for FMCW-SAR radars cannot be directly applicable.

In this paper, to design solutions for the motional frequency spread problem in wide-band FMCW automotive mmwave radars, we first model the IF signal and derive the analytical expressions of Doppler frequency interference term and the motion phase interference term caused by frequency spread. Based on these derivations, several effects of frequency spread, i.e., the degradation of range/velocity/angle estimation accuracy and range/velocity resolution, are comprehensively discussed with the help of numerical results. Motivated by the above analysis, we then propose three motional frequency spread calibration schemes with different performance and complexity tradeoff, which are inverse discrete Fourier transformation frequency calibration (IDFT-FC) scheme, spectrum cell rearrangement (SCR) scheme, and simple frequency correction (SFC) scheme. Finally, we construct a simulation platform for ADAS automotive mmwave radar systems based on practical system parameters. Simulations and complexity analysis show that the proposed IDFT-FC and SCR scheme can significantly improve the estimation accuracy of range/velocity/angle and the range/velocity resolution compared to the traditional scheme with no frequency spread calibration. Although the IDFT-DC scheme has better calibration performance, the SCR scheme provides a flexible tradeoff between performance and implementation cost. The SFC scheme can only improve the estimation accuracy of range and velocity but with nearly the same complexity as that of traditional schemes, i.e, its implementation cost is much lower than other proposed schemes.

To better clarify the novelty of our proposed schemes for wide-band automotive mm-wave radar, differences compared to the traditional compensation scheme in SAR are elaborated in the following from two aspects. With respect to the design purpose, the motion compensation scheme in SAR is to eliminate the effect of the Doppler frequency on the range/DOA estimation for improving the imaging quality [15], [16]. Instead of improving the imaging quality, the motion calibration in automotive mm-wave radar is mainly to improve the parameter estimation performance of interested targets with the effect of Doppler frequency spread on velocity estimation eliminated as well. With respect to the design mechanism, the SAR can utilize different but known relative velocity (between the target and the radar) in different relative orientations to compensate the motion in range-azimuth domain [14]. However, in automotive mm-wave radar, the corresponding calibration scheme should be designed in range-Doppler domain via exploiting the inner characteristics of the FMCW signal. The involved frequency spread mathematical form and compensation mechanism are then largely different from those in conventional SAR.

The remaining of the paper is organized as follows. Section II gives the echo signal model of the FMCW automotive mmwave radar systems. Section III provides analytical expressions of the Doppler frequency interference term and the motion phase interference term and shows the frequency spread phenomenon of the considered systems due to the relative motion between radar and target. In section IV, three calibration schemes are proposed for the problem of motional frequency spread. Section V shows simulations and conclusions are provided in Section VI.

II. FMCW SIGNAL MODEL

Fig. 1 shows the transmitted signal and echo of the FMCW radar. The amplitude of the transmitted signal is constant while its frequency varies linearly in each sweeping period. Consider the radar transmit signal of the m^{th} sweeping period

$$S_t(t,m) = rect\left(\frac{t-mT}{T}\right) \times exp\left[j2\pi f_0(t-mT) + j\pi\mu\,(t-mT)^2\right] \quad (1)$$

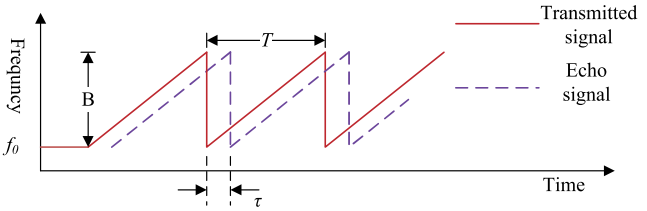

FIGURE 1. Transimitted and echo FMCW signal.

where t, T and f_0 are the signal time, the sweep interval and the center frequency, respectively. B is the sweeping bandwidth and $\mu = B/T$ is the frequency modulation rate. Using T as the interval, the signal can be denoted as a two-dimensional matrix with respect to range and velocity:

$$S_t(\hat{t}, t_s) = rect\left(\frac{\hat{t}}{T}\right) exp\left(j2\pi f_0 \hat{t} + j\pi\mu\hat{t}^2\right) \tag{2}$$

where $\hat{t} = t - mT$ and $t_s = mT$ are the signal time in the range and Doppler dimension, respectively.

Consider a target with a radial range r and a velocity v[1] when $t = 0$. Assuming that the target maintains an uniform linear motion relative to radar during the whole detection time, i.e., a coherent processing interval (CPI),[2] the echo delay caused by the radial range between the target and the radar is

$$\tau = \frac{2\left[r - v\left(\hat{t} + t_s\right)\right]}{c} \tag{3}$$

where c is the propagation speed of electromagnetic waves in free space. And the echo signal can be rewritten as:

$$S_r(\hat{t}, t_s) = rect\left(\frac{\hat{t} - \tau}{T}\right) \times exp\left[j2\pi f_0\left(\hat{t} - \tau\right) + j\pi\mu\left(\hat{t} - \tau\right)^2\right]. \tag{4}$$

By multiplying the echo signal with the conjugation of the transmitted signal, we have the IF signal as:

$$S(\hat{t}, t_s) = rect\left(\frac{\hat{t} - \tau}{T - \tau}\right) \times exp\left[j2\pi f_0\tau - j\pi\mu\tau^2 + j2\pi\mu\hat{t}\tau\right] \tag{5}$$

Substituting (3) into (5), we have

$$\begin{aligned} S(\hat{t}, t_s) = {} & rect\left(\frac{\hat{t} - \tau}{T - \tau}\right) exp\left[j2\pi\left(\frac{2\mu r}{c} - \frac{2vf_0}{c}\right)\hat{t}\right] \\ & \times exp\left[-j\frac{4\pi vf_0}{c}t_s\right] exp\left[-j\frac{4\pi\mu v}{c}(\hat{t} + t_s)\hat{t}\right] \\ & \times exp\left[-j\frac{4\pi\mu\left(r - v\left(\hat{t} + t_s\right)\right)^2}{c^2}\right] exp\left[-j\frac{4\pi rf_0}{c}\right]. \end{aligned} \tag{6}$$

[1] v is the radial velocity of the target relative to the radar, which is positive when the target is approaching.

[2] In practice, v may vary fast even in one CPI due to the acceleration or deceleration and/or angle changing between radar and targets, especially for the short-range automotive scenarios. Specific designs will be conducted in the future work.

The 1st exponential in (6) is the range frequency term which determines the target range. This term is influenced by the target velocity as well. The 2nd exponential in (6) is the Doppler frequency term, which is uniquely determined by the target velocity. The 3rd exponential in (6) is the motional frequency shift term which is caused by the relative motion between radar and target during the whole detection time. This term couples the time of range and Doppler dimension, which effects both range and Doppler frequency in FMCW automotive mmwave radar systems. This effect can be ignored for small μ and v. The 4th exponential in (6) is a high-order term of c, which has almost no influence on signal frequency and can also be ignored. The 5th exponential is a constant phase term with no effect on frequency.

Traditional FMCW automotive mmwave radar systems generally have narrow bandwidth and short detection time. Thus, the last three exponentials in (6) can be ignored. Therefore, the IF signal can be approximated as:

$$\begin{aligned} S(\hat{t}, t_s) \approx {} & rect\left(\frac{\hat{t} - \tau}{T - \tau}\right) exp\left[j2\pi\left(\frac{2\mu r}{c} - \frac{2vf_0}{c}\right)\hat{t}\right] \\ & \times exp\left[-j\frac{4\pi vf_0}{c}t_s\right]. \end{aligned} \tag{7}$$

Via using the two-dimension fast Fourier transformation (2D-FFT) processing for the signal in (7), we can obtain the range frequency and the Doppler frequency as

$$f_r = \frac{2\mu r}{c} - \frac{2vf_0}{c} \tag{8}$$

and

$$f_v = -\frac{2vf_0}{c} \tag{9}$$

respectively. The target range and velocity can be estimated from (8) and (9).

III. FREQUENCY SPREAD WITH WIDE-BAND FMCW

Self-driving in short-range scenarios requires a high range resolution for sensors. In FMCW automotive mmwave radar systems, the range resolution is uniquely determined and inversely proportional to the sweep bandwidth which is generally more than 1GHz [18]. Simultaneously, the radial velocity is more than 60m/s in large probability. Therefore, the 3rd exponential in (6) affects the range frequency and Doppler frequency due to the wide bandwidth for short range scenarios.

Recall that the 4th exponential in (6) is a high-order term of c which has a quite low influence on signal frequency in wide-band FMCW systems, and the 5th exponential in (6) is a constant phase term. Therefore, ignoring the 4th and 5th exponential in (6), the IF signal of wide-band FMCW can be approximated as:

$$\begin{aligned} S(\hat{t}, t_s) \approx {} & rect\left(\frac{\hat{t} - \tau}{T - \tau}\right) exp\left[j2\pi\left(\frac{2\mu r}{c} - \frac{2vf_0}{c}\right)\hat{t}\right] \\ & exp\left[-j\frac{4\pi vf_0}{c}t_s\right] exp\left[-j\frac{4\pi\mu v}{c}(\hat{t} + t_s)\hat{t}\right]. \end{aligned} \tag{10}$$

Via a Fourier transform in the Doppler time dimension, the signal in (10) becomes a narrow pulse with a *sinc* shape in the Doppler frequency dimension. The position of the pulse peak is

$$f_v = \frac{\partial\left[2\pi\left(\frac{2\mu r}{c}-\frac{2vf_0}{c}\right)\hat{t}-\frac{4\pi vf_0}{c}t_s-\frac{4\pi\mu v}{c}(\hat{t}+t_s)\hat{t}\right]}{2\pi\,\partial\hat{t}} = -\frac{2vf_0}{c}-\frac{2\mu v}{c}\hat{t}. \quad (11)$$

And the phase of this pulse is

$$\Phi_v = 2\pi\left[\left(\frac{2\mu r}{c}-\frac{2vf_0}{c}\right)\hat{t}\right]-2\pi\left(\frac{2\mu v}{c}\hat{t}^2\right). \quad (12)$$

It can be seen from (11) that the 2nd frequency term $-2\mu v\hat{t}/c$ is the Doppler frequency interference term, which is related to the range-dimension time. Therefore, the positions of the pulses in Doppler frequency dimension are distinct at different range-dimension times. Meanwhile, from (12), it can be seen that the 2nd phase term $-4\pi\mu v\hat{t}^2/c$ is a motion phase interference term, which is a quadratic term of the range-dimension time. This will affect the result of the Fourier transform in range dimension. Meanwhile, the peak position in range frequency dimension may shift beyond one or even more spectrum cells caused by the 3rd exponential in (6) due to the high range resolution, especially when the radial velocity of the target is high.

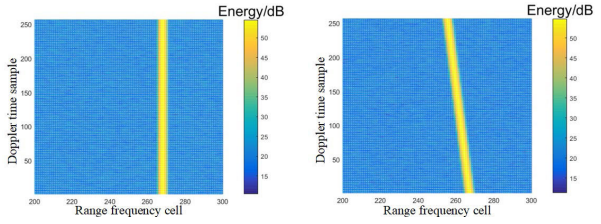

(a) Range dimension FFT result in stationary case (v=0m/s)
(b) Range dimension FFT result in high-velocity case (v=40m/s)

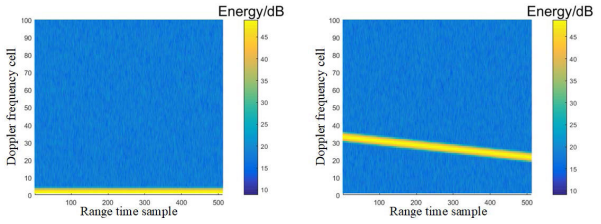

(c) Doppler dimension FFT result in stationary case (v=0m/s)
(d) Doppler dimension FFT result in high-velocity case (v=40m/s)

FIGURE 2. 1D-FFT results of wide-band FMCW IF signal.

For better clarification, Fig. 2 shows the one-dimension fast Fourier transformation (1D-FFT) results of wide-band FMCW IF signal in (6). Related system parameters are referred to Table 2 of Section V, and the SNR of echo signal is 10dB. It can be seen from Fig. 2(a) and 2(c) that when the relative velocity of target and radar is zero, the spectrum peaks are concentrated in the same location of range or Doppler dimension. This results from that the 3rd exponential in (6) equals to one and has no influence on frequency. However, in the high-velocity case (v = 40m/s), whether the fast Fourier transformation (FFT) processing is performed in range dimension or Doppler dimension first, as shown in Fig. 2(b) and 2(d), the location of spectrum peak in one dimension varies linearly along the other dimension since the effect of 3rd exponential in (6), i.e., the coupling term of range and Doppler dimension time, cannot be ignored. This variance will result in the frequency spreading as shown in the following.

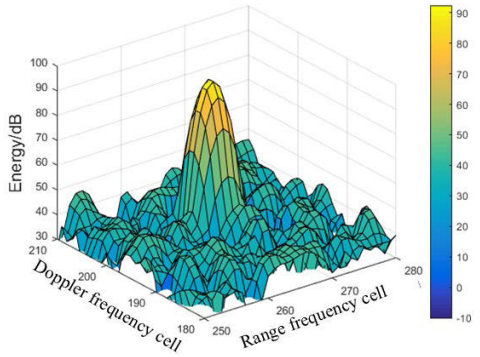

(a) 2D-FFT result in low-velocity case (v = 10m/s)

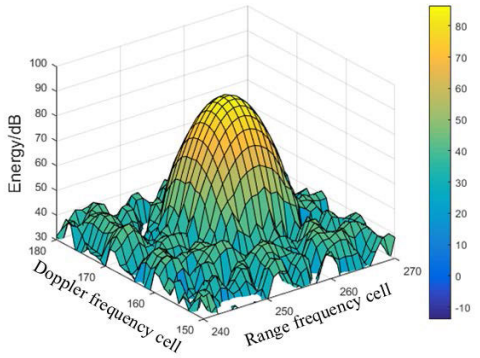

(b) 2D-FFT result in high-velocity case (v = 60m/s)

FIGURE 3. 2D-FFT results of wide-band FMCW IF signal.

Fig. 3 shows the 2D-FFT results of wide-band FMCW IF signal. Parameter settings are the same as those for Fig. 2 It can be seen that in the high-velocity (v = 60m/s) case, the spectral main lobe spreads severely and the value of peak energy is lower than that of the low-velocity (v = 10m/s) case. This frequency spreading results in many problems such as effective SNR loss and increasing of closely targets' mutual interference. To be more specific, Fig. 4 shows the results of FFT processing in range dimension for two closely located targets' wide-band FMCW IF signals where the radial range between targets and radar are 10m and 10.3m respectively and the rest parameters of these two targets are the same. The red dotted line in Fig. 4(b) denotes one certain range dimension spectrum cell which contains two targets' frequency signals due to the frequency spreading in the high

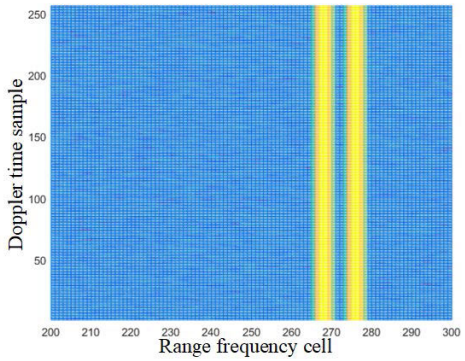

(a) 1D-FFT result of closely located targets' IF signal in stationary case

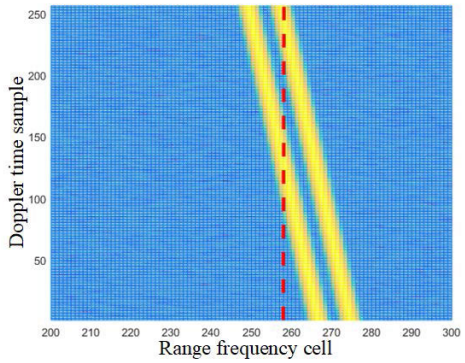

(b) 1D-FFT result of closely located targets' IF signal in high-velocity case

FIGURE 4. 2D-FFT results of wide-band FMCW IF signal.

velocity case ($v = 60$m/s). Thus these two closely located targets' mutual interference tends to increase and the system range/velocity resolution degrades. As shown in Fig. 4(a), the mutual interference is negligible in the stationary case.

Traditional FMCW automotive mmwave radar systems estimate the target range and velocity parameters directly using (8) and (9), according to the peaks' positions of the spectrum obtained from 2D-FFT processing. However, in the wide-band and/or high-velocity condition, the Doppler frequency interference term in (11) affects the Doppler frequency, so that the positions of spectrum peaks are distinct at different range-dimension times. Therefore, the echo energy is distributed on multiple spectrum cells in the Doppler frequency dimension. This results in the SNR loss, the increasing of closely spectrum cells' mutual interference and parameters estimation deviation. Therefore, it is necessary to correct the Doppler frequency shift in (11) and compensate the motion phase in (12) to eliminate the motional frequency spread problem in wide-band FMCW systems.

IV. CALIBRATION OF MOTIONAL FREQUENCY SPREAD

A. PHASE COMPENSATION

As described above, in wide-band FMCW systems, the motional frequency spread resulted from the relative target motion during the whole detection time causes the SNR loss, the increasing of closely located targets' mutual interference and parameters estimation deviation, and the degradation of range/velocity resolution. Therefore, it is necessary to correct and compensate the Doppler frequency interference term in (11) and the motion phase interference term in (12) to solve these problems.

It can be seen from (11) that different positions in Doppler frequency and range time dimension corresponds to different velocity values after performing FFT processing for the Doppler time dimension. Due to the property of frequency overlapping, the functional relationship is

$$V(\hat{t}, n_s) = \begin{cases} 0 & n_s = 1 \\ \dfrac{(N_s - n_s + 1)c}{2N_s T(f_0 + \mu\hat{t})} & n_s = 2, \ldots, N_s \end{cases} \tag{13}$$

where N_s is the FFT points in Doppler-frequency dimension. According to (12) and (13), for different positions in range time and Doppler frequency dimension, the phase compensation function is calculated as follow:

$$H(\hat{t}, n_s) = exp\left[j\frac{4\pi\mu V(\hat{t}, n_s)}{c}\hat{t}^2\right]. \tag{14}$$

Compensating the phase of FFT result in the Doppler-frequency dimension via multiplying the spectrum signal of different cells by (11), one can eliminate the influence of the relative motion between target and radar on the range-dimension Fourier transform.

For the Doppler frequency interference term in (11), two correction schemes are proposed in the next two subsections, i.e., the IDFT-FC scheme and the SCR scheme

B. IDFT-FC SCHEME

To make the Doppler frequency be only related to the target velocity rather than the range-dimension time. The same position of Doppler-dimension spectrum cell at different range-dimension times should corresponds to the same velocity. This needs the elimination of the influence of Doppler frequency interference term in (11), while keeping only the first Doppler frequency term. Therefore, we propose the IDFT-FC scheme with its detailed steps given in Algorithm 1. Denote the FFT results of IF signal in the Doppler dimension as $\boldsymbol{Y} \in \mathbb{C}^{N_q \times N_s}$ where N_s is the number of FFT points (including the filled zero points) and N_q is the sampling points of range dimension. After compensating the motion phase, the inverse discrete Fourier transform (IDFT) rotation factors are calculated according to the expected Doppler-dimension frequency corresponding to different positions of Doppler frequency and range time dimension. It can be derived from (11) that the expected Doppler frequency is

$$\bar{f_v} = -\frac{2vf_0}{c}. \tag{15}$$

And the IDFT rotation factor is

$$W(\hat{t}, n_s, m) = exp\left[j\frac{4\pi V(\hat{t}, n_s)}{c}f_0 mT\right], \quad m = 1, 2, \ldots, M \tag{16}$$

Algorithm 1 The IDFT Frequency Calibration (IDFT-FC) Scheme

1: For the IF signal of each receiving antenna of the system, fill in the zeros in the Doppler time dimension and perform the N_s-point FFT processing. The calculation result is $\boldsymbol{Y}$.
2: **for** $i = 1, 2, \ldots, N_q$ **do**
3: **for** $m = 1, 2 \ldots, M$ **do**
4: calculate $\check{\boldsymbol{Y}}[i][m] = \sum_{n_s=1}^{N_s} \boldsymbol{Y}[i][n_s] \times H\left(\frac{i}{N_q}T, n_s\right) \times W\left(\frac{i}{N_q}T, n_s, m\right)$
% the first multiplication is to compensate the phase interference in (12) and the second multiplication is to calibrate the frequency interference in (11)
5: **end for**
6: **end for**
7: For the IF time-domain signal $\check{\boldsymbol{Y}}$, perform the 2D-FFT processing and the subsequent FMCW automotive mmwave radar system signal processing.

where M is the number of sweep, i.e., the Doppler-dimension sampling points. Then, after performing the IDFT processing according to the IDFT rotation factor in (16), the two-dimension time-domain IF signal $\check{\boldsymbol{Y}} \in \mathbb{C}^{N_q \times M}$ with no influence of Doppler-frequency interference term can be obtained. Based on $\check{\boldsymbol{Y}}$, subsequent processing is the same as that of traditional scheme in FMCW automotive mmwave radar.

The IDFT-FC scheme can obtain an accurate two-dimension time-domain IF signal without the influence of motional frequency spread. This is because the IDFT can directly change the form of signal frequency by calculating the IDFT rotation factor corresponding to the expected Doppler frequency of each spectrum cell and then performing IDFT processing on it. This scheme achieves the optimal system performance if the effects of system resolution and noise can be ignored. However, since the rotation factor frequency interval is not constant, the butterfly structure of IFFT can no longer be used to accelerate the processing. Thus, this scheme requires a relative large amount of computational complexity.

C. SCR SCHEME

Motivated by the above mentioned computational complexity problem of IDFT-FC, a low-complexity frequency calibration scheme, i.e., the SCR scheme, is proposed in this subsection. For the Doppler dimension FFT result of IF signal, this SCR scheme is to rearrange the positions of spectrum cells according to the corresponding velocity values. The object of rearrangement is to ensure that after the motion phase compensation, the same positions of Doppler-dimension spectrum cells for different range time dimension samples corresponds the same velocity. This is because the rearrangement of the cellsAlo also changes the component of different frequencies in the IF signal. Compared with the IDFT-FC scheme, this scheme requires less computation and can directly perform the FFT processing on the rearranged result in the range time dimension without IDFT processing.

Algorithm 2 The Spectrum Cell Rearrangement (SCR) Scheme

1: For the IF signal of each receiving antenna, fill in the zeros in the Doppler time dimension and perform the N_s-point FFT processing. The calculation result is $\boldsymbol{Y}$.
2: Calculate the velocity resolution according to the system parameters $\Delta v = \frac{c}{2TMf_0}$.
3: **for** $m = 1, 2, \ldots, M$ **do**
% calculate the new Doppler frequency dimension coordinates from the velocity resolution and the sampling frequency in Doppler dimension
4: $\boldsymbol{V}[m] = (m-1)\Delta v$
5: **end for**
6: **for** $i = 1, 2, \ldots, N_q$ **do**
7: **for** $m = 1, 2 \ldots, M$ **do**
% for each cell in range time and new Doppler frequency dimension, find the closest velocity value among the different positions of Doppler frequency dimension with the same position of range time dimension
8: find $z = \arg\min_{n_s} \left| V\left(\frac{i}{N_q}T, n_s\right) - \boldsymbol{V}[m] \right|$, $n_s \in \{1, 2, \ldots, N_s\}$
% compensate the phase and fill in the corresponding cell of range time and new Doppler frequency dimension
9: $\bar{\boldsymbol{Y}}[i][m] = \boldsymbol{Y}[i][z] \times H\left(\frac{i}{N_q}T, n_s\right)$ *% Step 8 and Step 9 are to calibrate the frequency interference in (11) and the multiplication in Step 9 is to compensate the phase interference in (12)*
10: **end for**
11: **end for**
12: For rearrangement and phase compensation based $\bar{\boldsymbol{Y}}$, perform FFT processing in range time dimension directly and the subsequent FMCW automotive mmwave radar system signal processing.

The detailed steps of the proposed SCR scheme is given in Algorithm 2. For the IF signal of each receiving antenna, we perform N_s-point FFT processing in the Doppler-time dimension with zero-padding processing. Then, the velocity resolution is calculated according to the system parameters as the new coordinates of Doppler frequency dimension. For each cell in range time and new Doppler frequency dimension, the unit with the closest velocity value among the different positions of original Doppler frequency dimension with the same range time is found and filled in with the phase compensation. Finally, for the result after rearrangement and phase compensation (denoted as $\bar{\boldsymbol{Y}} \in \mathbb{C}^{N_q \times M}$), FFT processing in range time dimension can be performed directly along with the same following signal processing as that in the traditional scheme.

TABLE 1. The complexity of three proposed schemes.

Scheme	Additional multiplications	Additional complex storage
IDFT-FC	$N_q \times N_s \times (M + 1/2 \times log_2 N_s)$	$O(1)$
SCR	$1/2 \times N_q \times N_s \times [(L-1)log_2 N_s + L \times log_2 L]$	$O[(L-1) \times N_q \times N_s]$
SFC	2	$O(1)$

For the Doppler frequency domain signal, the SCR scheme performs position rearrangement to ensure that the spectrum cells with the same velocity value have the same positions at different range-dimension times, thus reducing the influence of Doppler frequency interference term. The SCR scheme requires no additional IDFT processing and the FFT processing can be directly performed for the rearranged results in the range time dimension. Compared with the IDFT-FC scheme, the SCR scheme has lower computation complexity, while the performance is dependent on the FFT spectrum interval size of Doppler dimension. In other words, the SCR scheme can achieve the same performance as the IDFT-FC scheme when enough zero-padding points are available in the Doppler dimension.

Although the SCR scheme has relative small computational complexity than the IDFT-FC scheme, the involved computation and storage may still be unaffordable for some low-cost systems. In the following subsection, the SFC scheme with quite low implementation complexity is proposed which requires almost no additional storage and negligible computation complexity increment compared with conventional signal processing procedure with no motion calibration.

D. SFC SCHEME

To simplify the engineering implementation, we propose an approximate correction scheme for the functional relationship between range/velocity frequency and range/velocity value in the parameter estimation module of the wide-band FMCW systems.

Via Fourier analysis for the range dimension of the system IF signal in (10), if the quadratic term of the range dimension signal time is ignored, the signal becomes a narrow pulse with a *sinc* shape in the range-frequency dimension with the pulse position being

$$f_r = \frac{\partial\left[2\pi\left(\frac{2\mu r}{c} - \frac{2vf_0}{c}\right)\hat{t} - \frac{4\pi v f_0}{c}t_s - \frac{4\pi\mu v}{c}(\hat{t}+t_s)\hat{t}\right]}{2\pi\,\partial\hat{t}} \approx \frac{2\mu r}{c} - \frac{2vf_0}{c} - \frac{2\mu v}{c}t_s \approx \frac{2\mu r}{c} - \frac{2vf_0}{c} - \frac{\mu v MT}{c}. \quad (17)$$

It can be seen from (17) that the pulse in range frequency dimension has distinct positions at different Doppler-dimension times. Therefore, we take the frequency value of the discrete FFT spectrum cell involving most spectrum peaks as an approximation of the target range frequency. The location should be closest to the average range frequency at different Doppler-dimension times.

Alternatively, the Doppler frequency value of the discrete FFT spectrum cell with most spectrum peaks is also approximated as the target Doppler frequency. From (11), the approximate Doppler frequency can be calculated as

$$f_v = -\frac{2vf_0}{c} - \frac{2\mu v}{c}\hat{t} \approx -\frac{2vf_0}{c} - \frac{\mu v}{c}T \approx -\frac{2vf_0}{c} - \frac{Bv}{c}. \quad (18)$$

Compared to traditional schemes in FMCW automotive mmwave radar systems, the SFC scheme uses the frequency approximation of the range/Doppler dimension frequency spread in (17) and (18), to substitute the corresponding function of the range/velocity value and range/Doppler frequency in (8) and (9).

The SFC scheme reduces the effect of the 3rd exponential in (6) on the system range/velocity estimation performance by correcting the corresponding function of range/velocity value and frequency. Different from the IDFT-FC and SCR schemes, the SFC scheme needs no additional signal processing compared with the traditional scheme. However, the problem of motional frequency spread is coarsely solved by the SFC scheme, and performance gap compared with other two proposed schemes may be non-negligible, e.g., the problems of SNR loss and mutual interference increasing still remain.

E. COMPLEXITY ANALYSIS

Table 1 shows the complexity of the three proposed calibration schemes for motional frequency spread, where the number of zero-padding points is L times the sampling points. It can be seen that compared with traditional signal processing procedure, the IDFT-FC scheme introduces the highest additional computation complexity, but only needs to have an additional storage of $O(1)$. Compared with IDFT-FC, the SCR scheme generally has lower computation complexity but an increased storage requirement. The additional storage demand is determined by the number of zero-padding points. The additional computation and storage introduced by the SFC scheme are negligible.

V. NUMERICAL RESULTS AND DISCUSSIONS

A simulation platform of the FMCW automotive mmwave radar systems is built as follows, where system parameters as shown in Table 2 are all referred to those in typical 77 GHz automotive radar chips. The SNR is defined for raw time-domain data. The simulations compare the three proposed schemes and the traditional scheme with no frequency spread calibration, and verify the effectiveness of the proposed designs.

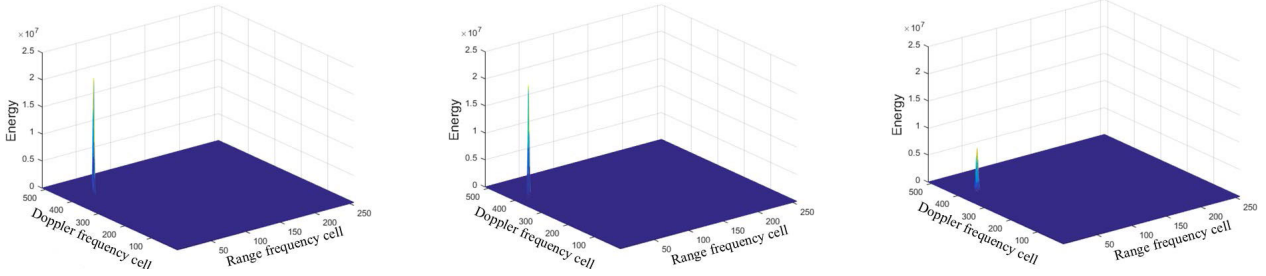

(a) Incoherent accumulation of 2D-FFT result in the IDFT-FC scheme

(b) Incoherent accumulation of 2D-FFT result in the SCR scheme

(c) Incoherent accumulation of 2D-FFT result in the traditional scheme

FIGURE 5. 2D-FFT results of wide-band FMCW IF signal.

TABLE 2. System parameters.

Parameter	Value	Parameter	Value
Center Frequency	77GHz	Sampling Rates	12MHz
Sweep Bandwidth	4GHz	Sampling points in range dimension	512
Zero-padding points in SCR	768	Sampling points in Doppler dimension	256
maximum detectable range	19.2m	sweep time	42.67μs
coherent processing interval	10.9ms	Velocity	$[0\text{m/s}, 40\text{m/s}]$
Field Angle	$[-50°, 50°]$	Antenna array	1×8
SNR	$[-32\text{dB}, -10\text{dB}]$		

Fig. 5 shows the incoherent accumulations of 2D-FFT results with different schemes, where $r = 10$m, $v = 40$m/s, $SNR = -10$dB, and the direction of angle (DOA) is the normal direction of the antenna. From Fig. 5, it can be seen that the IDFT-FC scheme has the highest peak energy of the two-dimension frequency domain. This means that the IDFT-FC scheme has the best performance in solving the problem of SNR loss in wide-band FMCW systems. Meanwhile, the peak energy in the SCR scheme with zero-padding processing is slightly lower than the IDFT-FC scheme. Both the IDFT-FC scheme and the SCR scheme are effective in solving the problem of SNR loss. In contrast, the SFC scheme has the same energy value as the traditional scheme since it only corrects the functional relationship between the range/velocity value and range/Doppler frequency in the parameter estimation module, and the problem of energy dispersion remains.

Fig. 6 and Fig. 7 show the range and velocity resolution of different schemes, respectively. The SNR of closely located targets are both -10dB. For the range resolution as shown in Fig. 6, the two targets have the same DOA (antenna normal direction), the same velocity value (40m/s), but the different range values (10m and 10.1m). Fig. 7 shows the velocity resolution where the range values are all 10m and the velocity values are 40m/s and 40.5m/s, respectively. The remaining parameters are the same as those in Fig. 6. Compared with the traditional scheme, the IDFT-FC scheme has better range/velocity resolution in high-velocity case. This verifies that the IDFT-FC scheme can improve the resolution in wide-band FMCW automotive mmwave radar systems. This improvement is also achievable for the proposed SCR scheme and the related demonstration is omitted here. And the SFC scheme has the same resolution as the traditional scheme since it only corrects the functional relationship between the parameter value and the frequency after the object detection module.

Fig. 8, Fig. 9 and Fig. 10 show the performance of parameter estimation in different schemes with different SNR, and the system parameters are shown in Table 2. It can be seen from Fig. 8 and Fig. 9 that the zero-padding SCR scheme has similar average error in range and velocity estimation to the IDFT-FC scheme. In addition, the SFC scheme has higher estimation error, but the performance degradation is not large in the considered settings. On the other hand, the traditional scheme without motional frequency spread calibration has an order of magnitude higher average error compared to the proposed three schemes in terms of range and velocity estimation. The average error of range and velocity estimation in three proposed schemes is in the centimeter level while that of traditional scheme is in the decimeter level. The proposed three motional frequency spread calibration schemes reduce the average error of the range and velocity estimation by more than 95% compared with the traditional scheme.

Fig. 10 shows the average error of angle estimation with different schemes and SNR. The adopted spatial spectrum estimation algorithm is ROOT-MUSIC algorithm [19]. As shown in Fig. 10, the IDFT-FC scheme can achieve the optimal angle estimation performance in the whole

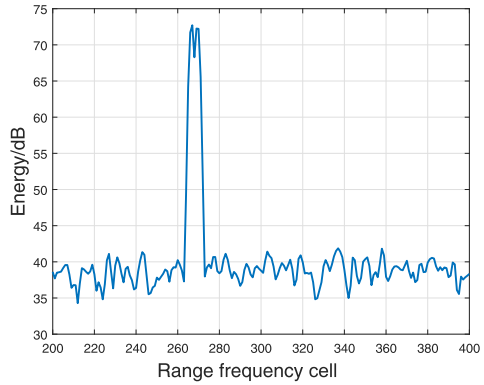

(a) Range resolution of IDFT-FC scheme

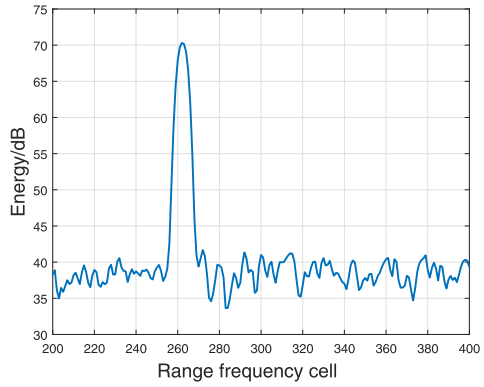

(b) Range resolution of traditional scheme

FIGURE 6. Range resolution of different scheme.

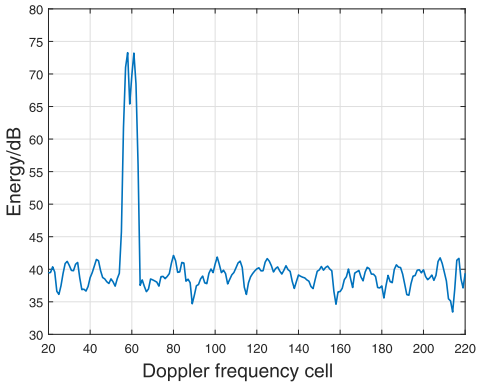

(a) Velocity resolution of IDFT-FC scheme

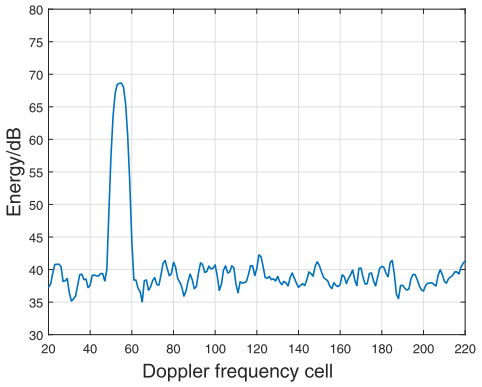

(b) Velocity resolution of traditional scheme

FIGURE 7. Velocity resolution of different schemes.

SNR range, and the average error is slightly less than the zero-padding SCR scheme. The traditional scheme without frequency spread calibration has significantly higher average error of angle estimation in the whole SNR range. This is because that both the proposed two schemes can reduce the motional frequency spread and the SNR loss in the two-dimension frequency domain. Besides, the SFC scheme only corrects the functional relationship between the range/velocity value and range/velocity frequency in the parameter estimation module and the motional frequency spread problem has not been fundamentally improved. Therefore, the SFC scheme has the same average error of angle estimation as the traditional scheme which is omitted in the figure.

For the more practical case of varying velocity during the detection time, Fig. 9 also shows the worst case velocity estimation performance with dotted lines, where the target acceleration is set to be 6m/s^2. It can be seen that the proposed schemes still effectively improve the velocity estimation performance compared with the conventional scheme. On the other hand, the average error of range and DOA estimation in varying velocity case are nearly the same as that in the constant velocity (omitted in the simulation), since the target range shift in the worst case during the coherent processing interval is 0.3 mm and this brings negligible SNR loss. The above performance

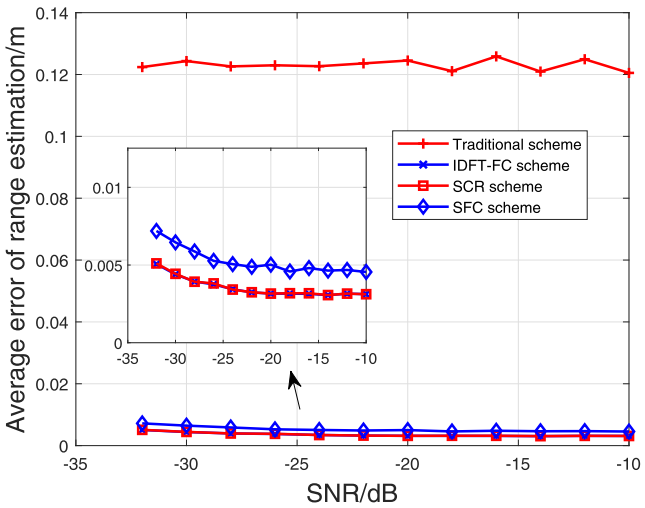

FIGURE 8. Average error of range estimation with different schemes and SNR.

validation can be extended to other practical propagation channels, e.g., the multiple-target case and scenarios with clutters. Although some performance degradation is inevitable due to interference from other targets and/or clutters, the main conclusion that the proposed schemes outperform traditional schemes remains. Simulation details are omitted here.

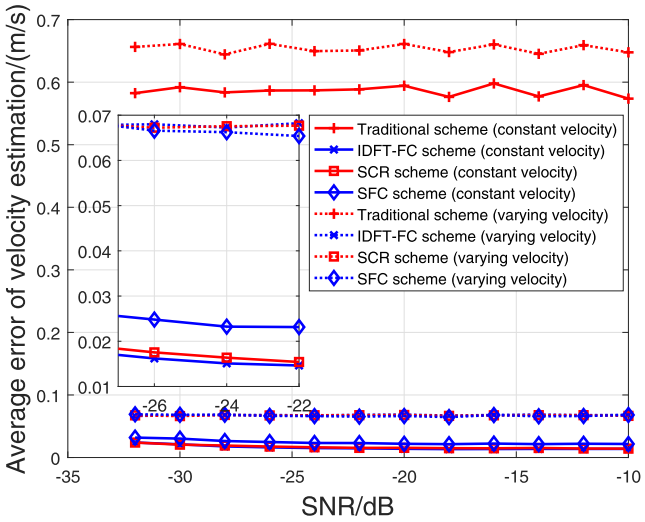

FIGURE 9. Average error of velocity estimation with different schemes and SNR.

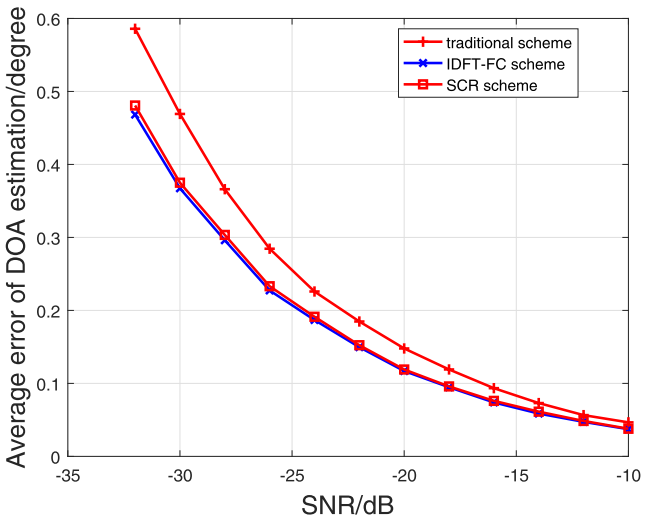

FIGURE 10. Average error of DOA estimation with different schemes and SNR.

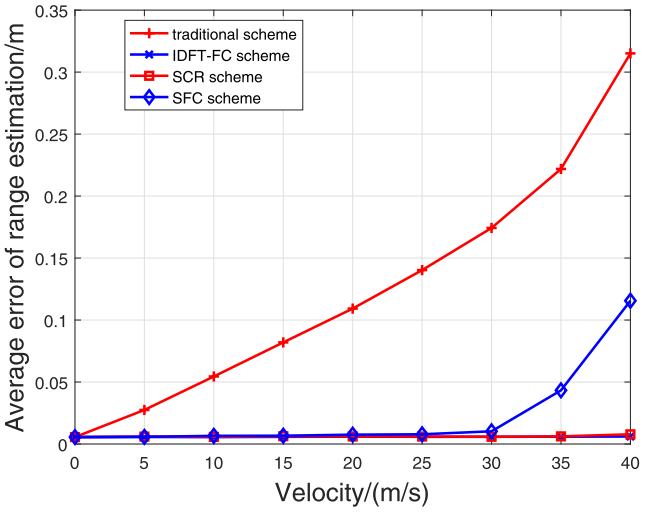

FIGURE 11. Average error of range estimation with different schemes and velocities.

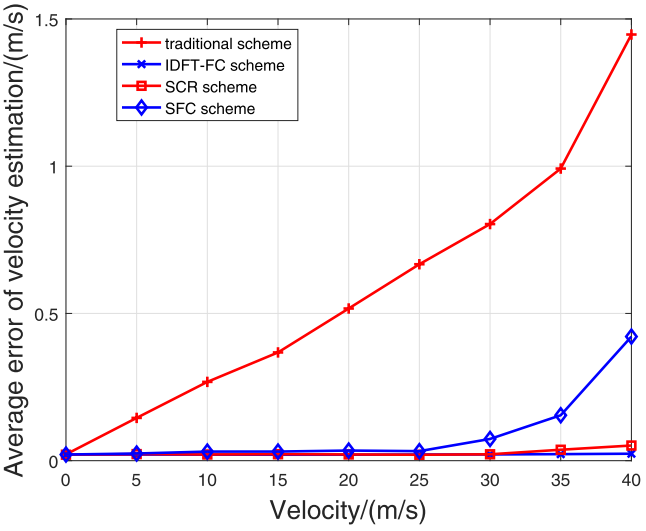

FIGURE 12. Average error of velocity estimation with different schemes and velocities.

Fig. 11, Fig. 12, and Fig. 13 show the performance of parameter estimation with different schemes and velocities. Considering the worst-case SNR for short range, the SNR of the echo signal is set to be -34dB. It can be clearly seen from the above three figures that the traditional scheme has the same estimation performance as these three proposed schemes when the relative velocity of target and radar is zero. In this stationary case, the 3rd exponential in (6) has no effect on the signal frequency or phase. As the velocity increases, the average error of the parameter estimation with the traditional scheme increases obviously which is nearly four times higher than that of low-velocity, especially when the velocity reaches 40m/s. The average error of the velocity estimation reaches the level of meter-per-second in high-velocity interval which can result in a serious performance degradation. In contrast, the IDFT-FC scheme has the optimal parameter estimation performance in the whole velocity interval, and the performance is independent of velocity. This verifies that the IDFT-FC scheme can effectively solve the motional frequency spread problem in wide-band FMCW systems. Meanwhile, compared with the IDFT-FC scheme, the zero-padding SCR scheme has almost the same performance of parameter estimation in low-velocity interval and a slightly higher average error in high-velocity interval.

As shown in Fig. 11 and Fig. 12, the SFC scheme is superior to the traditional scheme in estimating the value of range and velocity in the whole velocity range, and the performance gap becomes larger as the velocity increases. It shows that the SFC scheme can partially solve the problem of range/velocity estimation deviation caused by the frequency spread. Meanwhile, in the low-velocity interval ($v \leq 25$m/s), the average range/velocity estimation error of the SFC scheme is similar to those of IDFT-FC and SCR schemes. However, in the

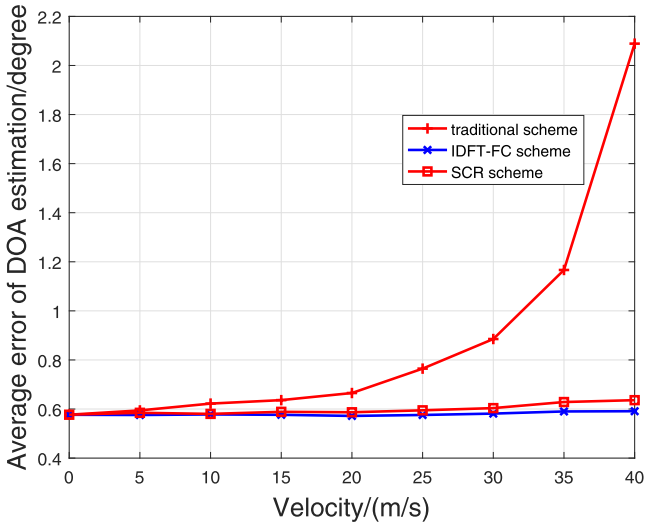

FIGURE 13. Average error of DOA estimation with different schemes and velocities.

high-velocity interval ($v > 25$m/s), as the velocity increases, the performance of the SFC scheme degrades faster. This is because that the SFC scheme only considers the frequency value corresponding to the most concentrated position of spectrum peaks in the entire range of frequency spread. And, in this way, the SFC scheme can achieve certain improvement in the low-velocity case, but the average error inevitably increases with frequency spread increasing.

Above simulation results show that 1) The traditional scheme without frequency spread calibration has the worst performance in the wide-band FMCW automotive mmwave radar systems and the system performance degrades in both range/velocity/angle estimation and range/velocity resolution, especially in high velocity case. 2) The IDFT-FC scheme has the optimal system performance, and the performance is independent of velocity. 3) The system performance of zero-padding SCR scheme is slightly lower than that of IDFT-FC scheme. The SCR scheme with 3 times zero-padding points has only about 6% computational complexity of the IDFT-FC scheme, but the requirement of storage is increased by 3 times. It is possible to improve the performance of the SCR scheme via increasing the zero-padding points in the FFT processing of the Doppler dimension within the storage limit. 4) The SFC scheme has the worst system performance among the three proposed schemes, but the improvement of the range/velocity estimation performance is obvious with negligible computation and storage increment, compared to the traditional scheme.

VI. CONCLUSION

In this paper, the motional frequency spread problem introduced by the relative motion of target and radar was studied for wide-band FMCW automotive mmwave radar systems. First, the approximate analytical expressions were derived for Doppler frequency shift and motion phase interference terms resulted from frequency spread. And the effect of frequency spread on system performance was analyzed, with respect to the estimation of range/velocity/angle and the resolution of range/velocity. Motivated by the above analysis, we proposed three motional frequency spread calibration schemes with different complexity and performance. Among them, the IDFT-DC scheme has the best system performance. The SCR scheme provides a flexible tradeoff between calibration performance and computational cost. The SFC scheme has negligible additional computation and storage compared to traditional schemes with no frequency spread calibration, but can only improve the performance of range/velocity estimation. For future work, motional frequency calibration design can be studied for the more complex non-point target.

REFERENCES

[1] M. Russell, A. Crain, A. Curran, R. Campbell, C. Drubin, and W. Miccioli, "Millimeter-wave radar sensor for automotive intelligent cruise control (ICC)," *IEEE Trans. Microw. Theory Techn.*, vol. 45, no. 12, pp. 2444–2453, Dec. 1997.

[2] J. Lee, Y.-A. Li, M.-H. Hung, and S.-J. Huang, "A fully-integrated 77-GHz FMCW radar transceiver in 65-nm CMOS technology," *IEEE J. Solid-State Circuits*, vol. 45, no. 12, pp. 2746–2756, Dec. 2010.

[3] J. Wenger, "Automotive radar–status and perspectives," in *Proc. IEEE Compound Semiconductor Integr. Circuit Symp. (CSIC)*, Palm Springs, CA, USA, 2005, pp. 21–25.

[4] H. Meinel, "Commercial applications of millimeterwaves: History, present status, and future trends," *IEEE Trans. Microw. Theory Techn.*, vol. 43, no. 7, pp. 1639–1653, Jul. 1995.

[5] I. Gresham, N. Jain, T. Budka, A. Alexanian, N. Kinayman, B. Ziegner, S. Brown, and P. Staecker, "A compact manufacturable 76-77-GHz radar module for commercial ACC applications," *IEEE Trans. Microw. Theory Techn.*, vol. 49, no. 1, pp. 44–58, 1st Quart., 2001.

[6] J. Hasch, E. Topak, R. Schnabel, T. Zwick, R. Weigel, and C. Waldschmidt, "Millimeter-wave technology for automotive radar sensors in the 77 GHz frequency band," *IEEE Trans. Microw. Theory Techn.*, vol. 60, no. 3, pp. 845–860, Mar. 2012.

[7] W. Wijesoma, K. Kodagoda, and A. Balasuriya, "Road-boundary detection and tracking using ladar sensing," *IEEE Trans. Robot. Automat.*, vol. 20, no. 3, pp. 456–464, Jun. 2004.

[8] S. M. Patole, M. Torlak, D. Wang, and M. Ali, "Automotive radars: A review of signal processing techniques," *IEEE Signal Process. Mag.*, vol. 34, no. 2, pp. 22–35, Mar. 2017.

[9] A. Stove, "Linear FMCW radar techniques," *IEE Proc. F Radar Signal Process.*, vol. 139, no. 5, p. 343, Oct. 1992.

[10] V. Winkler, "Range Doppler detection for automotive FMCW radars," in *Proc. Eur. Microw. Conf.*, Munich, Germany, 2007, pp. 166–169.

[11] E. H. Kim and K. H. Kim, "Random phase code for automotive MIMO radars using combined frequency shift keying-linear FMCW waveform," *IET Radar, Sonar Navigat.*, vol. 12, no. 10, pp. 1090–1095, Oct. 2018.

[12] A. Angelov, A. Robertson, R. Murray-Smith, and F. Fioranelli, "Practical classification of different moving targets using automotive radar and deep neural networks," *IET Radar, Sonar Navigat.*, vol. 12, no. 10, pp. 1082–1089, Oct. 2018.

[13] S. Lee, Y.-J. Yoon, J.-E. Lee, and S.-C. Kim, "Human–vehicle classification using feature-based SVM in 77-GHz automotive FMCW radar," *IET Radar, Sonar Navigat.*, vol. 11, no. 10, pp. 1589–1596, Oct. 2017.

[14] G. Xue, J. Yang, and P. Liu, "Modified range migration algorithm integrated with motion compensation for FMCW SAR," in *Proc. IET Int. Radar Conf.*, Xi'an, China, 2013, pp. 1–4.

[15] D. A. Ausherman, A. Kozma, J. L. Walker, H. M. Jones, and E. C. Poggio, "Developments in radar imaging," *IEEE Trans. Aerosp. Electron. Syst.*, vol. AES-20, no. 4, pp. 363–400, Jul. 1984.

[16] R. K. Raney, H. Runge, R. Bamler, I. G. Cumming, and F. H. Wong, "Precision SAR processing using chirp scaling," *IEEE Trans. Geosci. Remote Sens.*, vol. GRS-32, no. 4, pp. 786–799, Jul. 1994.

[17] S. Gishkori, L. Daniel, M. Gashinova, and B. Mulgrew, "Imaging for a forward scanning automotive synthetic aperture radar," *IEEE Trans. Aerosp. Electron. Syst.*, vol. 55, no. 3, pp. 1420–1434, Jun. 2019.

[18] V. Giannini, D. Guermandi, Q. Shi, A. Medra, W. Van Thillo, A. Bourdoux, and P. Wambacq, "A 79 GHz phase-modulated 4 GHz-BW CW radar transmitter in 28 nm CMOS," *IEEE J. Solid-State Circuits*, vol. 49, no. 12, pp. 2925–2937, Dec. 2014.
[19] B. D. Rao and K. V. S. Hari, "Performance analysis of root-music," *IEEE Trans. Acoust., Speech, Signal Process.*, vol. ASSP-37, no. 12, pp. 1939–1949, Dec. 1989.

CHENG ZHANG (Member, IEEE) received the B.Eng. degree from Sichuan University, Chengdu, China, in June 2009, the M.Sc. degree from the Xi'an Electronic Engineering Research Institute (EERI), Xi'an, China, in May 2012, and the Ph.D. degree from Southeast University, Nanjing, China, in December 2018. From June 2012 to August 2013, he was a Radar Signal Processing Engineer with Xi'an EERI. From November 2016 to November 2017, he was a Visiting Student with the University of Alberta, Edmonton, AB, Canada. He is currently an Assistant Professor with Southeast University (SEU), and supported by the Zhishan Young Scholar Program of SEU. He won the excellent Doctoral Dissertation of the China Education Society of Electronics, in December 2019. His research interests include space-time signal processing and machine learning for MIMO wireless communications and radar systems.

MENGDE CAO was born in Xuzhou, China, in 1994. He received the B.Eng. degree in communication engineering from Southwest Jiaotong University, Chengdu, China, in June 2016. He is currently pursuing the M.Sc. degree with Southeast University, Nanjing, China. His research interests include radar signal processing and learning algorithm in radar signal and data processing.

YUQIN GONG received the B.Eng. degree from the Nanjing University of Science and Technology, Nanjing, China, in June 2016. She is currently pursuing the M.Sc. degree with Southeast University, Nanjing. Her research interests include radar signal processing and target tracking in radar data processing.

YANG LI received the B.S. degree from Southeast University, Nanjing, China, in 2017, where he is currently pursuing the M.S. degree in information and communication engineering with the School of Information Science and Engineering. His current research interest is automotive millimeter wave radar signal processing.

YONGMING HUANG (Senior Member, IEEE) received the B.S. and M.S. degrees from Nanjing University, China, in 2000 and 2003, respectively, and the Ph.D. degree in electrical engineering from Southeast University, China, in 2007. Since March 2007, he has been a Faculty Member with the School of Information Science and Engineering, Southeast University, where he is currently a Full Professor. From 2008 to 2009, he visited the Signal Processing Laboratory, Electrical Engineering, Royal Institute of Technology (KTH), Stockholm, Sweden. His current research interests include MIMO wireless communications, cooperative wireless communications, and millimeter wave wireless communications. He has published over 200 peer-reviewed articles, holds over 60 invention patents. He submitted around 20 technical contributions to the IEEE Standards. He was awarded a certificate of appreciation for outstanding contribution to the development of the IEEE Standard 802.11aj.

HAIMING WANG (Member, IEEE) was born in 1975. He received the M.S. and Ph.D. degrees in electrical engineering from Southeast University, Nanjing, China, in 2002 and 2009, respectively. He joined the State Key Laboratory of Millimeter Waves, Southeast University, in April 2002. He is currently a Professor. In 2008, he was a short-term Visiting Scholar with the Blekinge Institute of Technology, Sweden. His current research interests include radio propagation measurement and channel modelling, signal processing for MIMO wireless communications, and millimeter-wave wireless communications. He received the First-Class Science and Technology Progress Award of Jiangsu Province of China, in 2009. He currently serves as the Vice Chair for the IEEE 802.11aj Task Group.